Phase transition and emergence of active temperature in an active Brownian system in underdamped background

Soumen De Karmakar* and Rajaraman Ganesh
Institute for Plasma Research, HBNI, Bhat, Gandhinagar, Gujarat 382428, India

(Received 12 September 2019; revised manuscript received 31 December 2019; accepted 27 February 2020; published 16 March 2020)

We explore the role of inertia in the properties of active Brownian particles (ABPs) immersed in an underdamped background in two dimensions using Langevin dynamics computer simulation. Similar to an equilibrium two-dimensional passive interacting particle system, the system of ABPs transits from a liquid phase to a solid phase with the change in the coupling parameter, which is the ratio of interaction potential energy and thermal energy of the background solvent. Important qualitative and quantitative differences are found in the liquid-solid phase transition with increasing strength of activity as compared to those found in the conventional overdamped background limit. In the underdamped background, inherent activity is found to lead to a temperature, called the *active temperature* and defined by average velocity fluctuations of the ABPs, that is different from the fixed background solvent temperature. A new scaling law for active temperature as a function of activity strength is found near the liquid-solid boundary. Active temperature, which behaves similar to the thermodynamic equilibrium temperature, is also found to depend upon the interaction strength between the active particles and the strength of the background dissipation. With an increase in background dissipation, the difference between active temperature and the background solvent temperature decreases and the difference is found to eventually vanish in the overdamped limit, demonstrating the correctness of the calculation.

DOI: 10.1103/PhysRevE.101.032121

I. INTRODUCTION

Active matter is a self-driven, out-of-equilibrium system consisting of motile entities which perform motion by consuming energy either from internal complex chemical processes or from their environment [1,2]. Unlike passive driven systems, viz., sheared glassy systems, vibrated granular matter, or complex plasma under gravity [3–5], active systems consume energy at the smallest possible length scale, i.e., at the individual particle length scale, and exhibit various kinds of complex phenomena, e.g., motility-induced phase transitions, large-scale dynamical patterns, and large fluctuations, to name a few [6–8].

The existence of effective temperature with a thermodynamic meaning in glassy systems is now well established [9,10]. A similar concept of effective temperature had successfully been applied in active systems both in simulation as well as in experiment [11,12]. Several attempts have been made to generalize thermodynamical concepts like free energy, and temperature in nonequilibrium active systems [13]. However, the prediction of effective temperature in an active system has been explored only to a limited extent [2]. Equilibrium-like critical phenomena, with near-equilibrium values of critical point exponents in certain specific types of active systems, had been reported [14]. In a recent work [15], the connection of irreversibility and an equilibrium second-law-like relation in an active colloidal system was reported. The existence of the equilibrium-like equation of state in a few models of active systems has been studied recently [16,17]. These works suggest that, despite their inherent nonequilibrium nature, active systems appear to obey equilibrium-like properties, to a certain extent, in the steady state.

In the study of self-motile or active Brownian particles (ABPs), microswimmers are, generally, immersed in a background solvent medium (for instance, water). The Reynolds number ($\mathrm{Re} = nlv/\mu$, where n and μ are the mass density and viscosity of the solvent, and l and v are the length scale and average speed of the microswimmers, respectively) for a system of ABPs turns out to be very low ($\mathrm{Re} \approx 10^{-4}$–$10^{-5}$) [2]. Consequently, the solvent (water) acts as a highly damping background for the ABPs (microswimmers). Hence, the inertial effects of the active particles could be neglected. In other words, inertia could be neglected (and is often neglected) when the relaxation time scale, which is inversely proportional to the viscosity of the background medium, is small compared to the time scale of the active particle dynamics. This limit of the system of ABPs is also known as the overdamped limit. Noninertial (overdamped) modeling also results in a reduction of computational work.

It is well known that a pure two-dimensional passive soft-disk system, confined in a periodic simulation box, transits from a liquid phase at high temperature (or low density) to a solid phase at low temperature (or high density) via a narrow hexatic region [18–20]. Liquid, hexatic, and solid phases are characterized by dynamical and structural properties of the system. For example, the solid phase is characterized by a relatively lower value of diffusion coefficient or higher structural ordering in comparison to that of the liquid phase. Recently, it was demonstrated that [21], despite the inherent activity,

*soumendekarmakar@gmail.com; soumen.dekarmakar@ipr.res.in

an active system in a two-dimensional periodic confining box can also be in a liquid or a solid phase (hexagonal structure) depending upon the density of the active entities. However, substantial differences are found between the liquid-solid transition of passive and active systems. Bialké *et al.* [21] showed that, in the overdamped limit, such transitions in active Brownian systems happen at different values of densities (coupling parameter) of the active entities for different measures of activity. It has also been demonstrated that there is an intermediate region between liquid and solid phases, different from the equilibrium hexatic phase, which is characterized by high structural order but with large structural fluctuations present due to inherent activity. It was also found that the phase area of the intermediate region increases with an increase in activity strength. Note that liquid-solid phase transitions are different from motility-induced phase transitions [6,22,23], one of the unique characteristics of an active system at relatively low density and high activity.

Moreover, it has been shown empirically that the effective temperature for a class of active systems, ranging from self-motile Brownian particles to active polymers, grows quadratically with activity strength [11,12]. Various independent measurements, obtained from a set of definitions ranging from deviations of an equilibrium fluctuation-dissipation relation to the kinetics of passive or driven tracer particles, follow the same quadratic relationship for the effective temperature. It was demonstrated recently [24] that the results of effective temperature obtained from many-body numerical simulations are consistent with analytic expressions that are derived for a single active particle in a viscoelastic liquid. These simulations were, mostly, performed in the liquid phase of the active systems in the overdamped limit.

In complete contrast to the overdamped case, where neglect of acceleration leads to lower-order differential equations and effective reduction in the phase space degrees of freedom, in the underdamped limit or inertia-included study, the phase space diagram is not truncated. In a recent study [25], it was demonstrated that the thermodynamics of a truncated or overdamped system underestimates the entropy production and the fluctuation theorem. Some of the recent studies [17,26,27] demonstrate the importance of inertia on the stress or pressure of active systems.

In the present work of a system of ABPs, we find qualitative and quantitative differences in the liquid-solid phase transition of ABPs in overdamped and underdamped background limits. We find, in the underdamped case, that the temperature of the ABPs, which originates from inherent activity, is different from that of the background bath temperature but with an increase in strength of the background dissipation; this difference reduces and eventually is found to vanish in the overdamped limit. We also demonstrate, qualitatively, the effect of interaction between the ABPs on their temperature. In the liquid phase, our results of quadratic dependence of temperature on the activity match with that of earlier works [12], but we find a new scaling law of the temperature of the ABPs with an increase in strength of the interaction between the active particles near the liquid-solid boundary. Our finding suggests that the temperature of the ABPs is a nonlinear function of activity, interaction strength, as well as the strength of the background dissipation.

II. SIMULATION MODEL

We study a colloidal suspension of N active particles immersed in a background solvent in two dimensions using the Langevin dynamics simulation [28,29]. The background solvent acts as the heat bath at constant temperature T. The Langevin equations for the ABPs are

$$\dot{\mathbf{r}}_i = \mathbf{v}_i, \tag{1}$$

$$m\dot{\mathbf{v}}_i = \mathbf{F}_i - \eta\mathbf{v}_i + \boldsymbol{\xi}_i + \mathbf{F}_i^a, \tag{2}$$

where $\mathbf{F}_i$ denotes total deterministic forces on the particle i. We consider pairwise repulsive Yukawa interaction between the ABPs,

$$u(r) = V_0\frac{e^{-r/\lambda}}{r}, \tag{3}$$

where V_0 and λ denote the strength and the range of the interaction potential, respectively. Then, the total conservative potential energy of the system is $U = \sum_{i<j} u(|\mathbf{r}_i - \mathbf{r}_j|)$. In general, $\mathbf{F}_i$ includes nonconservative external deterministic force as well but we consider no such force in this study. The time scale of the background molecules is much faster than that of the ABPs. The effect of the background is approximated by dissipative force $-\eta\mathbf{v}_i$ and fluctuating force $\boldsymbol{\xi}_i$. Here, η is the strength of the dissipation and $\boldsymbol{\xi}$ is the white Gaussian noise with zero mean and correlation $\langle\boldsymbol{\xi}_i(t)\boldsymbol{\xi}_j^T(t')\rangle = 2\eta k_BT\mathbf{I}\delta_{ij}\delta(t-t')$ [30], where $\mathbf{I}$ is the identity matrix and T is the background solvent temperature. $\mathbf{F}_i^a$ in Eq. (2) makes the system active [11,21]. It is modeled by a constant propelling force of magnitude f along the direction $\mathrm{e}_i(t) = \cos\theta_i(t)\hat{\mathbf{i}} + \sin\theta_i(t)\hat{\mathbf{j}}$ and overdamped rotational Brownian motion [31]

$$\dot{\theta}_i(t) = \zeta_i, \tag{4}$$

where ζ_i is δ-correlated Gaussian white noise like $\boldsymbol{\xi}_i$ but, unlike $\boldsymbol{\xi}_i$, the origin of ζ_i is the inherent motility of the ABPs. Correlation in ζ is given by

$$\langle\zeta_i(t)\zeta_j(t')\rangle = 2D_r\delta_{ij}\delta(t-t'), \tag{5}$$

where D_r is the free rotational diffusion coefficient of passive particles. For spherical particles of diameter σ, $D_r = 3D_0/\sigma^2$ [21], where $D_0 = k_BT/\eta$ is the diffusion coefficient of the passive Brownian particles in the absence of any interaction. Thus, $\mathbf{F}_i^a(t) = f\mathrm{e}_i(t)$. In our model, we neglect active friction, i.e., the damping effect associated with the active force $\mathbf{F}_i^a$ and any hydrodynamic effect due to activity. Thus, our model represents a situation of relatively low activity, where such effects are known to be negligibly small [15].

We use the units of mass (m), length ($\rho^{-1/2}$), and energy (k_BT), where m and ρ are the mass and number density of the ABPs, respectively, and T is the background solvent temperature, as the fundamental units in this study. Thus, the unit of time is $(m/\rho k_BT)^{1/2}$. In these units, Langevin equations [Eqs. (1) and (2)] become

$$\dot{\mathbf{r}}_i = \mathbf{v}_i, \tag{6}$$

$$\dot{\mathbf{v}}_i = -\boldsymbol{\nabla}_i\left(\Gamma\sum_{i<j}\frac{e^{-\kappa r_{ij}}}{r_{ij}}\right) - \gamma\dot{\mathbf{r}}_i + \boldsymbol{\xi}_i + f^a\mathrm{e}_i, \tag{7}$$

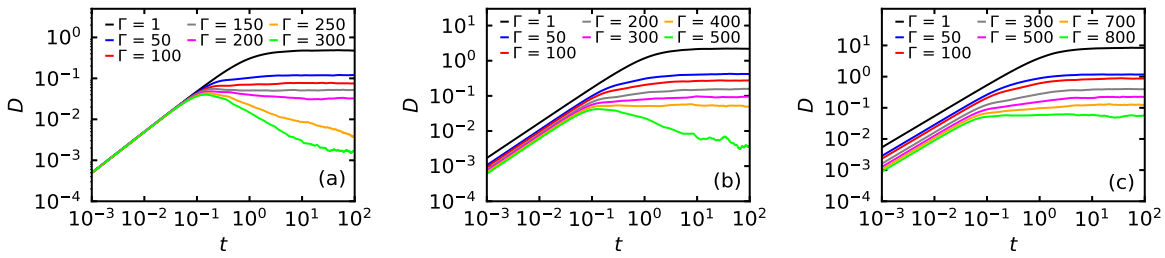

FIG. 1. Time-dependent diffusion coefficient D for passive (a) $f^a = 0$ and active (b) $f^a = 5$ and (c) $f^a = 10$ Brownian particles for different values of coupling strength Γ given in the legend.

where $\Gamma = V_0\rho^{1/2}/K_BT$ and $\kappa = \rho^{-1/2}/\lambda$ are the dimensionless coupling parameter and inverse screening length, respectively. The dimensionless white Gaussian noise $\boldsymbol{\xi}$ has the property of zero mean and correlation $\langle \boldsymbol{\xi}_i(t)\boldsymbol{\xi}_j(t')\rangle = 2\gamma \mathbf{I}\delta_{ij}\delta(t-t')$, where $\gamma = \eta/(m\rho k_BT)^{1/2}$ is the dimensionless dissipation strength. $f^a = f/\rho^{1/2}k_BT$ is the dimensionless active force strength. The correlation of ζ in dimensionless units becomes $\langle \zeta_i(t)\zeta_j(t')\rangle = 2\frac{D_r}{\gamma}\delta_{ij}\delta(t-t')$, where D_r denotes the dimensionless rotational diffusion constant. Note that in our unit, the background solvent temperature is $T = 1$.

In the limit of very high viscosity of the background solvent, the relaxation time scale (m/η) becomes much faster than the time scale associated with the ABPs $([m/\rho k_BT]^{1/2})$. Note that γ is the ratio of these two time scales; that is, $\gamma = \frac{(m/\rho k_BT)^{1/2}}{m/\eta}$. Hence, in this study, considering fixed masses m of all the active particles, an increase in background dissipation γ implies an increase in background viscosity η. Neglecting inertial effects at large γ results in the conventional overdamped Langevin equations for the ABPs [21],

$$\dot{\mathbf{r}}_i = -\frac{1}{\gamma}\left[\nabla_i\left(\Gamma\sum_{i<j}\frac{e^{-\kappa r_{ij}}}{r_{ij}}\right) + f^a\mathrm{e}_i + \boldsymbol{\xi}_i\right]. \tag{8}$$

III. SIMULATION DETAILS AND PARAMETERS

We perform a Langevin dynamics simulation, using Eqs. (6) and (7), by upgrading a well benchmarked molecular dynamics (MD) code MPMD [32,33] for this study. We consider $N = 1936$ particles, which is the same as the number of particles considered by Bialké *et al.* [21] in their phase transition studies in the overdamped limit. This choice will help us to compare our results with their overdamped results in the appropriate limit. We take a two-dimensional (2D) rectangular simulation box with dimensional ratio $L_x/L_y = 2/\sqrt{3}$ so that the system forms a perfect hexagonal crystalline state without any defect at high coupling strength Γ. Thus, the dimensions of our simulation box are $L_x \approx 47.28$ and $L_y \approx 40.95$. We apply periodic boundary conditions along both directions. The range of the interaction between the ABPs is controlled by κ in simulation. We take the value of $\kappa = 3.5$, which amounts to relatively short range interaction. We use the interaction cutoff $r_{\mathrm{cut}} = 4$ in our simulation. We choose the value of the rotational diffusion coefficient $D_r = 3.5$. We use the leapfrog time integrator with time steps $\Delta t = 10^{-4}$. The free parameters of our model are Γ, f^a, and γ.

We start from a random initial configuration and velocities, consistent with some arbitrary initial temperature. Langevin dynamics act as a thermostat. It takes the passive system ($f^a = 0$) to the background temperature $T = 1$ within a certain time depending upon the value of background dissipation γ. We evolve the system for a time $t = 50$, which is found to be long enough for all γ values used in this study. We then start to collect data for the desired values of our free parameters. Hence, our steady state results are produced using data from $t = 50$ onwards, which is shown as $t = 0$ in the figures [see Figs. 1 and 6(a)]. We repeat the same procedure five times with different initial states to perform an ensemble average. The above protocol is repeated for all the values of the free parameters (Γ, f^a, and γ). Whenever a comparison with the overdamped limit is required, we numerically solve the noninertial set of equations, Eq. (8). Otherwise, we evolve the system with full inertial equations, Eqs. (6) and (7).

IV. RESULTS

To understand the dynamical behavior, we study the diffusive properties. The noninteracting ($\Gamma \to 0$) passive ($f^a \to 0$) system shows normal diffusive behavior; i.e., in the large time limit, its mean square displacement (MSD) varies linearly with time. The diffusion coefficient D of such a two-dimensional system is given by [5]

$$D = \lim_{t\to\infty}\frac{1}{4t}\left\langle\frac{1}{N}\sum_{i=1}^{N}|\mathbf{r}_i(t) - \mathbf{r}_i(0)|^2\right\rangle, \tag{9}$$

where $\langle\cdots\rangle$ denotes the ensemble average. It is well known [33,34] that a highly correlated passive system shows super-, normal, and subdiffusive properties with an increase in coupling strength Γ. That is, the MSD of such a system, in general, does not vary linearly with time. However, the diffusion coefficient of such a system is obtained from the same relation as in Eq. (9) at a large time limit.

We plot $D(t)$ vs t for various parametric values of Γ for the passive system in Fig. 1(a) and for the active system with $f^a = 5$ and $f^a = 10$ in Figs. 1(b) and 1(c), respectively, in the underdamped limit with $\gamma = 1$.

With increase in activity strength f^a, the behavior of the system becomes more superdiffusive in nature, which is clear from the relatively smaller slopes of the logarithmic curves beyond the ballistic region.

We have taken a commensurate two-dimensional simulation box. Therefore, in the solid phase, the system of passive particles forms a hexagonal structure, that is, a triangular symmetric lattice, with six nearest-neighboring particles. We investigate the structural properties of our system by global

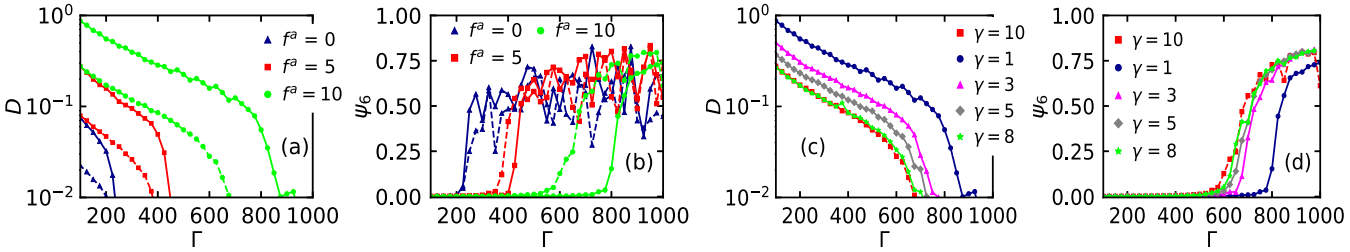

FIG. 2. (a) Long time diffusion coefficient D [Eq. (9)] vs coupling strength Γ and (b) global orientational order parameter ψ_6 vs Γ for different values of activity strength f^a given in the legend. Solid curves correspond to the inertial results in the underdamped cases with $\gamma = 1$ and the dashed curves correspond to the noninertial results in the overdamped cases with $\gamma = 10$. (c) D and (d) ψ_6 as a function of Γ for fixed activity $f^a = 10$. Solid curves correspond to the inertial results for various parametric values of dissipation strength γ and the dashed curve corresponds to the noninertial result at $\gamma = 10$.

bond-orientational order parameter ψ_6 [35],

$$\psi_6 = \langle | \frac{1}{N} \sum_{i=1}^{N} q_6(i) |^2 \rangle,$$

$$q_6(i) = \frac{1}{6} \sum_{j=1}^{N_6} e^{i6\theta_{ij}}, \tag{10}$$

where N_6 are the six nearest neighbors of the ith particle and θ_{ij} is the angle between the i and j particles with respect to some arbitrary fixed axis. The complex vector $q_6(i)$ (local bond-orientational order parameter) measures the local orientation of the ith particle in the complex two-dimensional plane. In the solid phase, due to the formation of the hexagonal structure, there is a large correlation between the local ordering of each particle. Now, due to thermal fluctuations, it is well known that even a two-dimensional system of passive particles does not form a perfect crystal. Hence, in the solid phase, the global orientational order parameter ψ_6 will give a high value but not ideally equal to 1. In the liquid phase, due to the random movement of the particles, there is no long range structural ordering between the particles. Hence, ψ_6 will give a low value (nearly zero).

In Figs. 2(a) and 2(b), we plot the diffusion coefficient D and global orientational order parameter ψ_6, respectively, as a function of coupling parameter Γ for three different values of activity strength: $f^a = 0$ (passive system), $f^a = 5$, and $f^a = 10$. Solid curves are the inertial results with dissipation constant $\gamma = 1$ and dashed curves are the noninertial results with $\gamma = 10$. From the nature of the curves, it is evident that active systems also move from a liquid phase to a solid phase with an increase in Γ. Both phases are characterized in more detail later. Interestingly, we find that there is a substantial shift of the underdamped results in comparison to the overdamped results along the Γ axis for each set of activity strength f^a and the difference increases with an increase in f^a. Moreover, the variation of the curves becomes more gradual near the transition region with an increase in activity, but the underdamped curves vary more drastically in comparison to the overdamped curves near the transition region for each set of f^a. Fluctuation in the solid phase [see Fig. 2(b)] is the signature of the thermal motion, which is evident from a low but nonzero value of diffusion [see Fig. 2(a)] of the ABPs. With the increase in statistics for ensemble averaging, these fluctuations are found to decay. In this study, we have considered five different initial configurations to perform the ensemble averaging for each data point. An increase in this number will increase the computational time. It is interesting to note that each point in Fig. 2(b), with 10 CPU cores, was found to consume about 40 min wall clock time. For about 41 points with five sets of such data, the estimated computational time for Figs. 2(b) and 2(d) is about 90 days. This brings out the computationally intensive nature of our calculations.

In Figs. 2(c) and 2(d), we plot D and ψ_6 as a function of Γ for fixed activity strength $f^a = 10$ and different parametric values of dissipation constant γ. Solid lines are the inertial results with increasing values of γ and the single dashed line is the noninertial result with $\gamma = 10$. It is evident from Figs. 2(c) and 2(d) that our underdamped results tend towards the overdamped results at large background dissipation.

We plot the phase diagram of both the overdamped and underdamped systems in Fig. 3. We obtain the curve $\Gamma^O_{\psi_6}$ for the overdamped case and the curve $\Gamma^U_{\psi_6}$ for the underdamped case from the equilibrium threshold criteria of $\psi_6 = 0.45$ (see Ref. [21]). These curves set the upper boundary of the liquid phase of our system of ABPs in the overdamped and the underdamped cases, respectively.

The liquid phase is characterized by a high value of diffusion and very low structural order in comparison to the

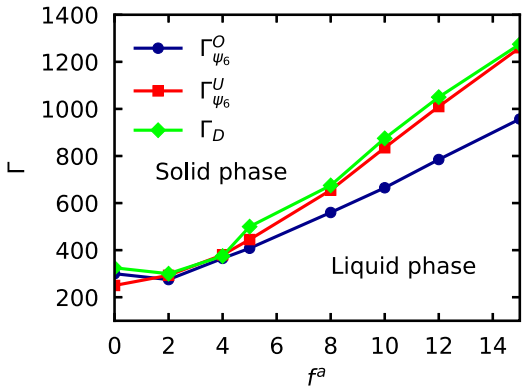

FIG. 3. Phase diagram of our system of ABPs. $\Gamma^O_{\psi_6}$ and $\Gamma^U_{\psi_6}$ curves are obtained from the equilibrium criteria of $\psi_6 = 0.45$ (see the main text) for overdamped and underdamped cases, respectively. The Γ_D curve is obtained from the critical values of the coupling parameter when the saturation of defects or hexagons is reached for different values of f^a (see the main text).

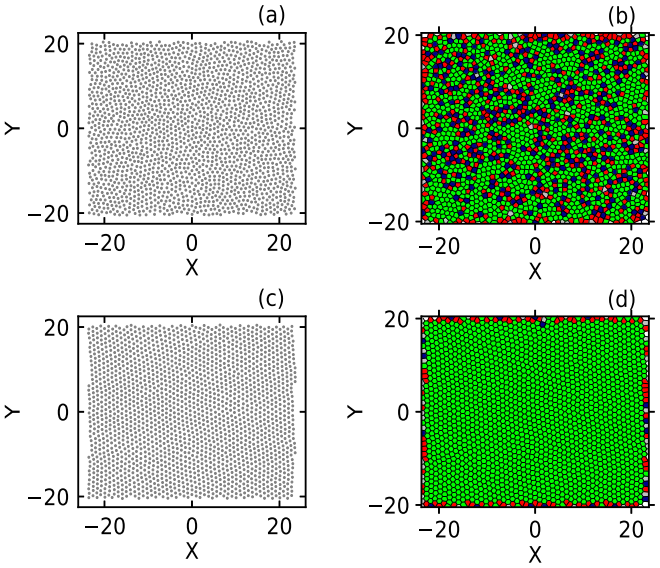

FIG. 4. (a) Configuration snapshot for $f^a = 10$ and $\Gamma = 500$ (liquid phase) and (b) the corresponding Voronoi plot. (c) Configuration snapshot for $f^a = 10$ and $\Gamma = 950$ (solid phase) and (d) the corresponding Voronoi plot. In the Voronoi plots, green (light grey) corresponds to hexagons (six nearest neighbors) and the other colors correspond to the defects: red (grey) corresponds to pentagons, blue (dark) corresponds to heptagons, and white corresponds to other defects and defects due to open polygons at the system boundaries.

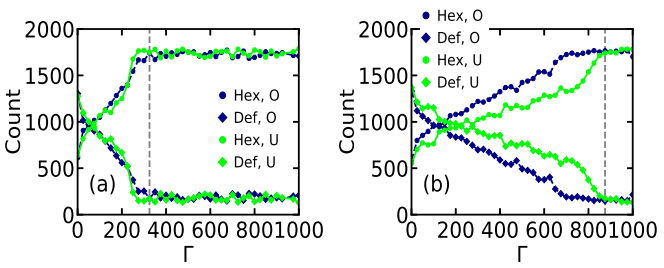

FIG. 5. Polygon count vs Γ for (a) $f^a = 0$ (passive system) and (b) $f^a = 10$. In the legend, "Hex" corresponds to hexagon count, "Def" corresponds to defect count, "O" corresponds to the noninertial results in the overdamped case with $\gamma = 10$, and "U" corresponds to the inertial results in the underdamped case with $\gamma = 1$. Dotted vertical lines give the value of Γ when the saturation values in the number of defects or hexagons are reached. We denote the critical value of Γ as Γ_D (see the main text).

solid phase. Consequently, there is a very low correlation between the local orientational order $q_6(i)$ corresponding to each particle i. In other words, in the liquid phase, there is very low triangular or hexagonal symmetry. To understand the local behavior of our active system, we have defined a *defect* [19] as the case when a particle does not have six nearest neighbors. In the liquid phase, we observe a large number of local isolated defects, but in the solid phase, we find very few defects and they are found (in the case when defects are present) to be in pairs of pentagon (a particle with five nearest neighbors) and heptagon (a particle with seven nearest neighbors), as found in equilibrium passive systems. A pentagon-heptagon pair is also called a *dislocation* [19]. In Figs. 4(a) and 4(b), we plot an instantaneous configuration snapshot and corresponding Voronoi diagram of our system of ABPs for $f^a = 10$ and $\Gamma = 500$ (liquid phase), and in Figs. 4(c) and 4(d), we plot an instantaneous configuration and Voronoi snapshot for $f^a = 10$ and $\Gamma = 950$ (solid phase). In the Voronoi plots, green (light grey) corresponds to hexagons (six nearest neighbors) and the other colors correspond to the defects [red (grey) corresponds to pentagon, blue (dark) corresponds to heptagon, and white corresponds to other defects and defect due to open polygons at the system boundaries].

If we plot the number of defects with coupling parameter Γ for a fixed activity strength f^a, we obtain a saturation value in the solid phase. Consequently, we also obtain a saturation value in the number of hexagons in the solid phase. In Figs. 5(a) and 5(b), we plot the number of hexagons and defects for $f^a = 0$ (passive case) and $f^a = 10$, respectively. Solid green (light gray) curves correspond to the underdamped and the dashed blue (dark) curves correspond to the overdamped results. The dotted vertical line gives the value of Γ when the saturation value in the number of defects or hexagons is reached. We denote the critical value of Γ as Γ_D. There is almost no difference between the overdamped and the underdamped results for the passive system ($f^a = 0$) but there is a substantial difference for the active system (f^a=10). We also observe that the saturation is reached almost at the same value of Γ_D for both the underdamped as well as the overdamped cases for the active system. The Γ_D line in our phase diagram corresponds to the critical values of the coupling parameter when the saturation of defects is reached for different values of activity strength f^a. Hence, the Γ_D line sets the lower boundary of the solid phase of our system of ABPs for both underdamped and overdamped cases.

Thus, we also observe an intermediate region, characterized by global order but local structural fluctuations present due to activity, in the overdamped case and the area of it increases with an increase in activity. This is the same result as found by Bialké *et al.* [21]. However, in the underdamped case of our system of ABPs, the intermediate region is found to vanish.

We now turn to another interesting observation regarding the temperature of the active Brownian system. In Fig. 1, diffusion vs time curves for different values of Γ for the ABPs do not overlap in the ballistic region but they do overlap for the passive particles. It is important to note that we start to collect data after a sufficiently long time ($t = 50$). Within that time, we expect that Langevin dynamics take the system to the background temperature. Thus, we expect the curves to overlap in the ballistic region for the active system, as observed in the case of passive particles. This apparent paradox suggests that there could be a temperature for the system of ABPs, different from that of the background solvent.

To address this curiosity, we start with the average random kinetic energy per particle in our unit as

$$E_K = \frac{1}{2N}\sum_{i=1}^{N}(\mathbf{v}_i - \langle\mathbf{v}\rangle)\cdot(\mathbf{v}_i - \langle\mathbf{v}\rangle), \tag{11}$$

where $\langle\mathbf{v}\rangle$ is the average velocity. For a passive system in equilibrium, the temperature is defined in terms of the average

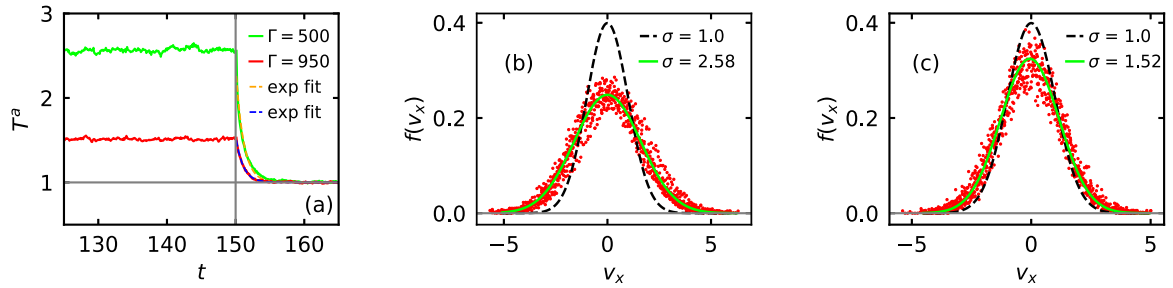

FIG. 6. (a) Active temperature T^a [Eq. (11)] vs time t for $\Gamma = 500$ and $\Gamma = 950$ and fixed activity strength $f^a = 10$. Self-force is switched off at $t = 150$. Dashed curves are the exponential fit (see main text). The horizontal solid line at $T^a = 1$ denotes the background solvent temperature. Velocity distribution (x component of velocity, v_x) data, from $t = 140$ to $t = 150$ with time interval $\Delta t = 1$ between two data sets, of the ABPs with $f^a = 10$ and (b) $\Gamma = 500$ and (c) $\Gamma = 950$ are shown with red dots. Solid curves are the Gaussian fit with (b) mean $\mu = 0$ and variance $\sigma = 2.58$ and (c) $\mu = 0$ and $\sigma = 1.52$. For reference, Gaussian distributions with $\mu = 0$ and $\sigma = 1$ corresponding to the background solvent are shown by black dashed curves in (b) and (c).

random kinetic energy per particle in the limit $N \to \infty$ through the equipartition theorem. We adopt the same kinetic definition of temperature for ABPs [28] of finite number and call it the *active temperature* T^a. Therefore, in our unit, $E_K \equiv T^a$.

In Fig. 6(a) we plot T^a vs t for fixed activity strength $f^a = 10$ and fixed dissipation strength $\gamma = 1$ for two different values of coupling strength, $\Gamma = 500$ (liquid phase) and $\Gamma = 950$ (solid phase) (see Fig. 3). The background solvent temperature is denoted by the horizontal solid line at $T = 1$. It is evident that for the active system ($f^a = 10$) T^a is different from that of the background temperature $T = 1$ in both liquid and solid phases. In the liquid phase, temperature, as well as fluctuations, is higher than in the solid phase. At $t = 150$ we turn off the activity ($f^a = 0$), thereby making the particles passive. The temperature of the ABPs quickly converges to the background solvent temperature $T = 1$ for both values of Γ. We fit the data with an empirical relation $T^a(t) = ae^{-bt} + c$ after switching off the activity. The dashed lines in Fig. 6(a) are the fitted curves with the values of the fit parameters $(a, b, c) \approx (1.381, 0.906, 1.001)$ for $\Gamma = 500$ and $(a, b, c) \approx (0.551, 0.936, 1.001)$ for $\Gamma = 950$, respectively. For both values of Γ, the parameter b has almost the same value to within numerical accuracy. Hence, it is obvious that the fall does not depend upon Γ; it only depends upon γ, i.e., the relaxation time scale.

We plot the velocity distribution (x component of the velocities, v_x) of the ABPs for $(f^a, \Gamma) = (10, 500)$ in Fig. 6(b) and for $(f^a, \Gamma) = (10, 950)$ in Fig. 6(c). The solid curve in both Figs. 6(b) and 6(c) is Gaussian fit with mean and variance $(\mu, \sigma) \approx (0, 2.58)$ and $(\mu, \sigma) \approx (0, 1.52)$, respectively. The dashed curve in the velocity distribution plots is Gaussian with $\mu = 0$, $\sigma = 1$. We obtain similar results for the y component of velocity (v_y) as well. Note that we have defined the temperature (active temperature T^a) of our model system of nonequilibrium active Brownian particles, borrowing an equilibrium definition of temperature (proportional to the fluctuations of the particles). The origin of the active temperature is the inherent activity of the ABPs; however, T^a is found to follow an equilibrium-like Gaussian distribution in steady state.

In Fig. 7(a) we plot T^a vs f^a for $\gamma = 1$ and three different values of coupling parameter, $\Gamma = 175$, $\Gamma = 500$, and $\Gamma = 950$, respectively, with the solid curves. Note that for $\Gamma = 175$ the system is well inside the liquid phase for all values of activity. We fit the data with an empirical relation $T^a = 1.0 + b(f^a)^{2+\alpha}$. Fitted curves are plotted with dashed lines in Fig. 7(a). Values of α are 0.104, 0.413, and 1.249 for $\Gamma = 175$, 500, and 950, respectively. Hence, we find that the quadratic dependence of T^a on activity strength, as obtained in some of the earlier work [11,12,24], is mostly limited to the liquid phase. As one approaches the liquid-solid boundary,

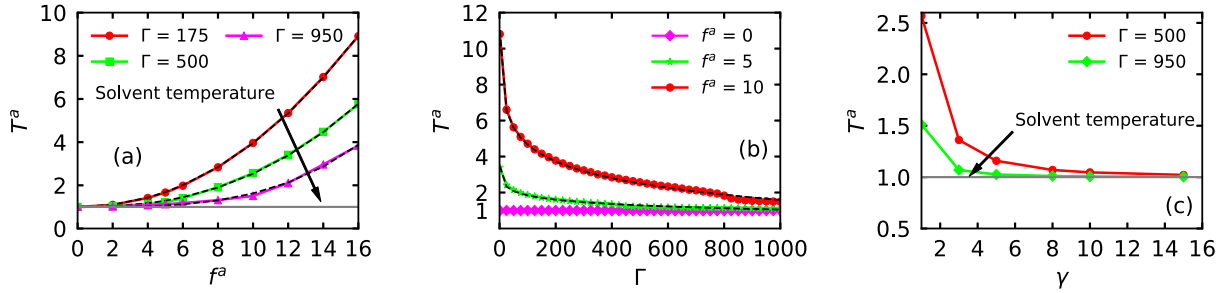

FIG. 7. (a) Active temperature T^a vs activity strength f^a (solid curves) for three different coupling strengths Γ given in the legend. Dashed curves are the fitted curves to the empirical relation $T^a = 1.0 + b(f^a)^{2+\alpha}$ (see main text). (b) T^a vs Γ for different activity strength f^a given in the legend. $f^a = 0$ corresponds to the passive interacting system. Dashed curves are the fit to the empirical relation $T^a = b(1/\Gamma)^{0.01} + c$ with appropriate fit parameters b and c (see main text). (c) Inertial results for T^a vs dissipation strength γ for two different values of coupling strength Γ given in the legend. Activity is kept constant at $f^a = 10$. The horizontal solid line at $T^a = 1$ in (a), (b), and (c) corresponds to the constant background solvent temperature.

a new scaling, different from quadratic scaling, of T^a as a function of f^a is found to emerge.

To understand the role of coupling parameter Γ on the active temperature T^a, we plot in Fig. 7(b) T^a vs Γ for $\gamma = 1$ and three different values of activity strength, $f^a = 0$, $f^a = 5$, and $f^a = 10$, with the solid curves. For the passive system ($f^a = 0$), the temperature of the system is independent of Γ. The passive temperature is dictated only by the background solvent temperature. We fit our results with an empirical relationship $T^a = b(1/\Gamma)^{0.01} + c$. Fitted data are plotted with dashed curves, with fit parameters $(b, c) = (36.372, -32.892)$ and $(b, c) = (141.414, -130.388)$ for $f^a = 5$ and $f^a = 10$, respectively. Hence, we demonstrate that, for the active system, coupling plays an important role, as it tries to restrict the inherent fluctuations of the particles. Therefore, with an increase in coupling strength Γ, T^a diminishes.

In Fig. 7(c), we plot T^a as a function of background dissipation strength γ for two different values of coupling strength, $\Gamma = 500$ and $\Gamma = 950$, keeping the activity of the system fixed at $f^a = 10$. From Fig. 7(c), it is evident that the temperature of the system of ABPs, that is, the active temperature T^a, decays with an increase in background dissipation in both liquid and solid phases, and at very large values of background dissipation, T^a tends to converge to the background solvent temperature $T = 1$.

The reason for this behavior is the following: Dissipation takes the system into a dead state ($T = 0$), whereas background fluctuations keep the system alive, and they are connected by the fluctuation-dissipation relation. As a result, a passive system acquires background temperature after a sufficient time, determined by the relaxation time scale m/η. Now, active particles feed energy into the system on a time scale $(m/\rho k_B T)^{1/2}$. In the underdamped case, when the relaxation time scale and time scale in which active particles feed energy into the system are comparable, inertia plays an important role and the background solvent molecules do not get sufficient time to acquire, via interactions, the input energy due to activity. Eventually, it goes into the random component as active temperature T^a due to an interplay between the coupling parameter, inertial active dynamics, and the interaction of the background solvent molecules with the active particles. With the increase in dissipation strength η, i.e., with the decrease in relaxation time scale m/η, background effects start to dominate over the other effects and the background solvent tries to take away the input energy due to activity. In the limit of large dissipation that is in the overdamped limit, when the relaxation time scale becomes very small in comparison to the time scale of the active particles, inertial effects play practically no role and the background solvent takes away the input energy instantaneously. Hence, in the limit of high background dissipation, we obtain the temperature of the system of ABPs to be the same as that of the background solvent temperature.

V. DISCUSSION AND CONCLUSION

We have demonstrated that in the relatively low dissipative background, inertia plays an important role in the dynamical, structural, as well as thermodynamical properties of self-motile or active Brownian particles. In particular, we have demonstrated that the intermediate region between the liquid and solid phases, which is characterized by high structural order but with large structural fluctuations present due to activity (as found in earlier works), is found to vanish in underdamped background.

The system of active Brownian particles, at the low dissipative background, acquires a temperature, the active temperature T^a, which behaves similar to the equilibrium temperature, but the value of the active temperature is different from that of the background solvent temperature. The quadratic dependence of T^a on activity strength is found to be valid only in the liquid phase, in agreement with earlier work [11,12,24], whereas near the solid-liquid boundary T^a is found to follow a different scaling law from the quadratic scaling. Moreover, coupling plays an important role in the temperature of the active system as it tries to restrict the inherent fluctuations of the ABPs. In the overdamped limit, the relaxation time scale becomes very short and the background takes away the input energy due to motility, thereby making no difference between active and background temperature.

In complex plasmas or dusty plasmas [36], micron sized conducting or dielectric grains get negatively charged and interact with each other via Coulomb interaction, shielded by the ambient plasma medium. The temperature of this grain medium is easily controlled by grain-neutral collisions, which act as a "Brownian" background. The grain density, ambient plasma density, and neutral density are routinely controlled in laboratories [36], thus making it possible to go from underdamped to overdamped limits continuously. The grain particles, if styled as Janus particles, then become an active system that can go from inertia-less to an inertial limit [2]. In this kind of experimental setup, we believe that our findings reported here can be verified.

Furthermore, it would be interesting to study the system of active Brownian particles including explicit alignment interaction, the active damping effect associated with the active fluctuations, and external influence. Due to the scale associated with rotational inertia, in the inertial limit, rotational inertia can also play a major role [28,29,37] in the properties of ABPs. Hence, it would also be interesting to study the system of ABPs including inertia in rotational dynamics.

ACKNOWLEDGMENTS

This work has been carried out at the Institute for Plasma Research (IPR), Gandhinagar, India. Simulations for this work were carried out on UDAY and ANTYA clusters at IPR. The authors would like to thank the anonymous referees for their suggestion to include the phase diagram of our system and for pointing out several important references.

[1] S. Ramaswamy, Annu. Rev. Condens. Matter Phys. **1**, 323 (2010).

[2] C. Bechinger, R. Di Leonardo, H. Löwen, C. Reichhardt, G. Volpe, and G. Volpe, Rev. Mod. Phys. **88**, 045006 (2016).

[3] L. Berthier and J.-L. Barrat, Phys. Rev. Lett. **89**, 095702 (2002).
[4] A. Kudrolli, Rep. Prog. Phys. **67**, 209 (2004).
[5] H. Charan, R. Ganesh, and A. Joy, Phys. Plasmas **21**, 043702 (2014).
[6] M. E. Cates and J. Tailleur, Annu. Rev. Condens. Matter Phys. **6**, 219 (2015).
[7] E. Ben-Jacob, I. Cohen, and H. Levine, Adv. Phys. **49**, 395 (2000).
[8] S. Ramaswamy, J. Stat. Mech. (2017) 054002.
[9] H. A. Makse and J. Kurchan, Nature (London) **415**, 614 (2002).
[10] G. D'Anna, P. Mayor, A. Barrat, V. Loreto, and F. Nori, Nature (London) **424**, 909 (2003).
[11] D. Loi, S. Mossa, and L. F. Cugliandolo, Phys. Rev. E **77**, 051111 (2008).
[12] D. Loi, S. Mossa, and L. F. Cugliandolo, Soft Matter **7**, 10193 (2011).
[13] S. C. Takatori and J. F. Brady, Phys. Rev. E **91**, 032117 (2015).
[14] M. Han, J. Yan, S. Granick, and E. Luijten, Proc. Natl. Acad. Sci. USA **114**, 7513 (2017).
[15] L. Dabelow, S. Bo, and R. Eichhorn, Phys. Rev. X **9**, 021009 (2019).
[16] S. Das, G. Gompper, and R. G. Winkler, Sci. Rep. **9**, 6608 (2019).
[17] Y. Fily, Y. Kafri, A. P. Solon, J. Tailleur, and A. Turner, J. Phys. A: Math. Theor. **51**, 044003 (2017).
[18] E. P. Bernard and W. Krauth, Phys. Rev. Lett. **107**, 155704 (2011).
[19] W. Qi, A. P. Gantapara, and M. Dijkstra, Soft Matter **10**, 5449 (2014).
[20] S. C. Kapfer and W. Krauth, Phys. Rev. Lett. **114**, 035702 (2015).
[21] J. Bialké, T. Speck, and H. Löwen, Phys. Rev. Lett. **108**, 168301 (2012).
[22] T. Hanke, C. A. Weber, and E. Frey, Phys. Rev. E **88**, 052309 (2013).
[23] R. Großmann, L. Schimansky-Geier, and P. Romanczuk, New J. Phys. **14**, 073033 (2012).
[24] S. Kumar Nandi and N. S. Gov, Eur. Phys. J. E **41**, 117 (2018).
[25] A. Celani, S. Bo, R. Eichhorn, and E. Aurell, Phys. Rev. Lett. **109**, 260603 (2012).
[26] S. C. Takatori and J. F. Brady, Phys. Rev. Fluids **2**, 094305 (2017).
[27] M. Joyeux and E. Bertin, Phys. Rev. E **93**, 032605 (2016).
[28] S. Mandal, B. Liebchen, and H. Löwen, Phys. Rev. Lett. **123**, 228001 (2019).
[29] M. Sandoval, Phys. Rev. E **101**, 012606 (2020).
[30] R. Zwanzig, *Nonequilibrium Statistical Mechanics* (Oxford University Press, Oxford, UK, 2001).
[31] N. Van Kampen, *Stochastic Processes in Physics and Chemistry* (Elsevier Science, Amsterdam, 2011).
[32] Ashwin J. and R. Ganesh, Phys. Rev. Lett. **104**, 215003 (2010).
[33] H. Charan, Ph.D. thesis, HBNI, Institute for Plasma Research, 2017.
[34] Z. Donkó, J. Goree, P. Hartmann, and B. Liu, Phys. Rev. E **79**, 026401 (2009).
[35] H. Lowen, J. Phys.: Condens. Matter **4**, 10105 (1992).
[36] G. E. Morfill and A. V. Ivlev, Rev. Mod. Phys. **81**, 1353 (2009).
[37] C. Scholz, S. Jahanshahi, A. Ldov, and H. Löwen, Nat. Commun. **9**, 5156 (2018).